

RESEARCH

Open Access



Resistance Behaviours of Clamped HFR-LWC Beam Using Membrane Approach

Wanxiang Chen^{1,2,3}, Jiawen Cai¹, Junxuan Huang¹, Xiaoyu Yang¹ and Jianjun Ma^{1,3*}

Abstract

Beam-like members sustaining the combined action of transverse load and membrane force exhibit a special load response to progressive deflection. A theoretical model is therefore developed to depict the resistance behaviours of clamped reinforced concrete (RC) beams observed in tests. The support-induced membrane effects are simulated by a longitudinal spring and a rotational spring. The load responses to progressive deflection are obtained using the membrane approach, and the prediction accuracies of proposed method are validated by a series of four-point bending tests on hybrid fibre reinforced-lightweight aggregate concrete (HFR-LWC) beam. It is illustrated that the bearing capacities of clamped HFR-LWC beam are significantly enhanced by the membrane effect. Ultimate load of the clamped beam ranges from 64.0 to 184.0 kN, and the larger bearing capacity compared with simply supported beam is obtained. An ultimate load of 1.85 to 5.31 times the yield line value is achieved, and thereby, the ultimate resistance of the clamped beam might be seriously underestimated using yield line approach. A strong support constraint is beneficial for increasing the load-carrying capacity of clamped HFR-LWC beam, although the large longitudinal restraint stiffness would inevitably gives rise to brittle failure. The relative errors between predicted load and measured value are less than 7.23%, indicating that the presented model is a promising tool to estimate the ultimate load of clamped beam-like member.

Keywords HFR-LWC beam, Membrane action, Bearing capacity, Prediction model, Experimental study

1 Introduction

Resistance function is essential for structural dynamic analysis. The resistance behaviours of RC beams or one-way slabs (i.e., beam-like members), as well as analytical methods, have caught great interest from people involved in civil engineering during the 1940s and 1960s. The yield-line theory proposed by Johansen (1962)

in 1943 is a common and powerful tool to estimate the ultimate resistances of RC beam-like members and was subsequently explained and developed by other scholars (Gamble, 2000; Hognestad, 1953).

Generally, the yield line approach provides an adequately accurate result for engineering applications (Park & Park, 1975). However, tests performed by Ockleston (1955) demonstrated that the bearing capacities of clamped slabs considerably exceeded those estimated using yield-line models (Wood et al., 1970), which was later confirmed by many structural experiments (Brotchie & Holley, 1971; Park, 1964a, 1964b). It was found that the notable increases in resistance were raised by the membrane effect, namely, a restraint to longitudinal movement and edge-rotation given by the adjacent frame. Recently, the resistance behaviours of clamped members have been studied intensively. The ultimate resistances of a heated concrete floor slab under bending load

Journal information: ISSN 1976-0485 / eISSN 2234-1315.

*Correspondence:

Jianjun Ma
majianjun@mail.sysu.edu.cn

¹ School of Civil Engineering, Sun Yat-sen University, and Southern Marine Science and Engineering Guangdong Laboratory (Zhuhai), Zhuhai 519082, China

² State Key Laboratory of Disaster Prevention & Mitigation of Explosion & Impact, Army Engineering University of PLA, Nanjing 210007, China

³ State Key Laboratory for Tunnel Engineering (Sun Yat-sen University), Guangzhou 510275, China



© The Author(s) 2023. **Open Access** This article is licensed under a Creative Commons Attribution 4.0 International License, which permits use, sharing, adaptation, distribution and reproduction in any medium or format, as long as you give appropriate credit to the original author(s) and the source, provide a link to the Creative Commons licence, and indicate if changes were made. The images or other third party material in this article are included in the article's Creative Commons licence, unless indicated otherwise in a credit line to the material. If material is not included in the article's Creative Commons licence and your intended use is not permitted by statutory regulation or exceeds the permitted use, you will need to obtain permission directly from the copyright holder. To view a copy of this licence, visit <http://creativecommons.org/licenses/by/4.0/>.

accompanying membrane action induced by restrained thermal expansion were analysed by Martin Gillie et al. (2004). Bailey (2000, 2001) presented a new analytical approach to describe the behaviours of membrane action in lightly reinforced concrete slabs, and a simple design equation was also presented to predict the ultimate resistance of an unrestrained slab subjected to membrane action at large displacements. The tensile membrane action of lightly reinforced thin concrete slabs at large deflections was investigated by Burgess (2017), illustrating that the tensile membrane force acted as an enhancement in fire conditions and substantially degraded the contribution of steel beams. The membrane actions in slabs of steel-structure buildings under fire conditions were investigated by Li et al. (2007). An improved model was proposed by Chen et al. (2014) to estimate the ultimate resistance of flexibly supported RC members, and it was further used to depict the load responses of RC beams under dynamic loading. In addition, the contributions of membrane action on the load-carrying capacities of HFR-LWC beams were experimentally investigated by the author, demonstrating that the safety factor of 1.5 to 2.0 recommended in the current design code was not reasonable (Chen et al., 2021). Apparently, the potential safety reserve in the existing design manuals must be re-defined using membrane approach.

Seeking a new building material with high specific strength is the inevitable purpose of structure engineering. Lightweight aggregate concrete (LWC) is a newly developed material because of its advantageous mechanical and physical properties (Zhou et al., 2016). Nevertheless, its popularization in civil engineering is limited by the lower tension-to-compression ratio and significantly poor ductility (Libre et al., 2011; Wang & Wang, 2013). Fibres are commonly incorporated to improve the performance (i.e., ductility and tensile strength) of LWCs (Li et al., 2017a; Mo et al., 2017; Wang & Wang, 2013). The “hybrid effect” of various fibres on LWC was deeply explored (Hou et al., 2007; Kayali et al., 2003; Libre et al., 2011; Pan et al., 2011; Wang et al., 2014), and the positive effect of hybrid fibres was quantitatively described. The hybrid effect on the toughness of pumice LWC raised by steel fibres and polypropylene fibres was investigated by Libre et al. (2011). Additionally, the behaviours of Forta-Ferro and steel fibre-reinforced LWCs were studied by Nematzadeh et al. (2017). With respect to structural component, Sabetifar et al. (2021) presented a semi-empirical model to estimate the ultimate shear capacity of steel fibre-reinforced concrete beams using gene expression programming technique. The flexural behaviours of bilayer steel fibrous concrete beams with GFRP rebars was experimentally inspected by Fallah-Valukolae et al.

(2022), results showed that the flexural properties of concrete beams increased by adding 0.75% steel fibres. Nevertheless, per the same fibre ratio, bilayer fibrous beams had weaker flexural performance relative to one-layer fibrous concrete beams. An extensive investigation was conducted for the combined effect of crumb rubber aggregates and steel fibres on shear behaviour of GFRP bar-reinforced high-strength concrete beams (Nematzadeh et al., 2021). It was found that the steel fibres were more efficient in improving the beam shear behaviour at higher content of crumb rubber, such that they changed the cracking type and failure mode from shear to flexural. The feasibility of improving the flexural performance of beams with lap-spliced bars after exposure to heat by incorporating hybrid steel-polypropylene fibres was studied by Hossain-Zada et al. (2023), it is found that the addition of fibres improved the energy absorption and ductility of the heated and unheated specimens. Currently, LWC beams or one-way slabs are widely used as frame members and bridge decks owing to their excellent specific strength, and longitudinal movement and edge rotation are prevented by supports during service time. However, we lack knowledge about the resistance behaviours of HFR-LWC members accompanying membrane action. It is significant to reasonably estimate the ultimate load of clamped HFR-LWC beam and give an exact resistance function for its practical application.

Although the factor relevant to membrane action can sometimes provide a conservative reference for engineering designs, membrane contribution can no longer be accepted as a safety reserve, and attention must be given to more precise definitions of the resisting mechanism. In this paper, the resistance behaviours of clamped HFR-LWC beams are theoretically investigated, and the reliabilities and prediction accuracies of proposed method are well supported by the experimental studies conducted by author.

2 Load responses of Clamped Member

As shown in Fig. 1, the longitudinal elongation and the edge-rotation of clamped beam are restricted by the supports. The longitudinal force N and the resisting moment M associated with progressive deflection might result in complex failure mechanisms and considerable ultimate resistances over the yield line value (Chen et al., 2020; Johansen, 2004; Krauthammer, 2008). Consequently, the clamped member would experience a special deflection-dependent load response to its collapse, as described by the author in Chen et al. (2021), including a compressive-membrane stage and a tensile-membrane stage, as displayed in Fig. 2.

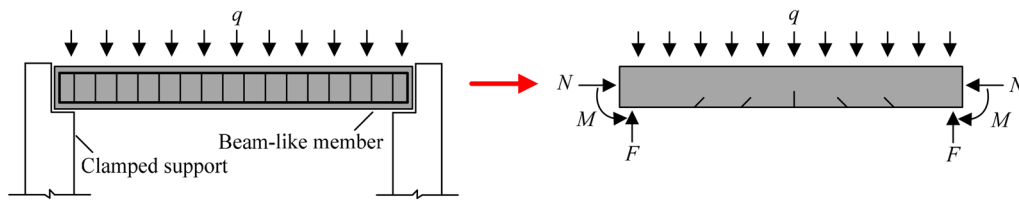


Fig. 1 Schematic of clamped member

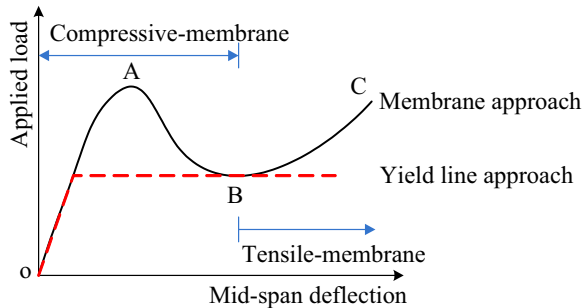


Fig. 2 Load-responses of clamped member

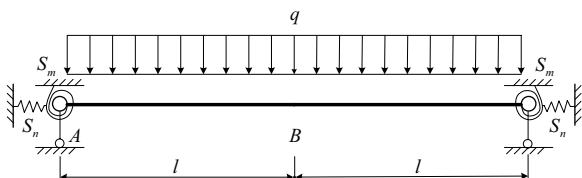


Fig. 3 Theoretical schematic for clamped beam

3 Resistance Model of Clamped RC Beam

Longitudinal elongation and edge-rotation of beam-like members are prevented by the supports with comparable stiffness, resulting in a notable resistance increase and special failure mode compared with simply supported beams (i.e., membrane effect) (Qian & Wang, 2009). Theoretically, the clamped beam can be regarded as a simply supported beam with a flexible constraint (Chen & Guo, 2010). Generally, the flexible constraint is characterized by a longitudinal spring and a rotational spring (see Fig. 3), where q is the transverse load, l is the half-span of the beam, S_n is the longitudinal restraint stiffness, and S_m is the rotational restraint stiffness.

Usually, as shown in Fig. 4a, the clamped beam collapses with three plastic hinges at a full span (Krauthammer, 2008): two plastic inflections form at the supports, followed by a mid-span plastic inflection as the external load continues. Therefore, the collapsed beam is composed of two straight rigid bodies connected by the mid-span plastic inflection (Park, 1964b). As shown in Fig. 4b, a half-span span of beam AB is

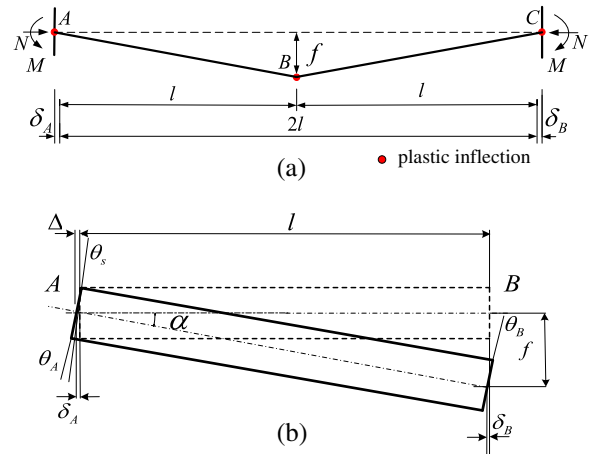


Fig. 4 Geometric graph of deformed beam: **a** global view; **b** local view

taken as the analysis segment. The geometric equation of global deformation for segment AB can be expressed as:

$$(l - \delta_A - \delta_B + \Delta)^2 + f^2 = [(1 - \varepsilon)l]^2 \quad (1a)$$

$$f = \alpha l \quad (1b)$$

$$\alpha = \theta_A + \theta_s = \theta_B \quad (1c)$$

where f is the deflection of mid-span Section B ; Δ is the horizontal movement of Section A ; ε is the average compression strain of segment AB ; δ_A and δ_B are the horizontal movements of Sections A and B detaching from their original position, respectively; θ_A and θ_B are the average rotation angles of Sections A and B , respectively; θ_s is the rotation angle of flexible support; and α is the angle of neutral axis between deformed segment and its original position.

A reduction factor is introduced to account the decrease in section height owing to the top crushed concrete (Shen et al., 1993). There are $\delta_A = \eta^A h \theta_A$ and $\delta_B = \eta^B h \theta_B$, and then Eqs. (1a, 1b, 1c) can be re-written as:

$$(\eta^A + \eta^B)h\frac{f}{l} - \eta^A h\theta_s = \frac{f^2}{2l} + \varepsilon l + \Delta \tag{2}$$

where h is the original height of the cross-section.

It is well known that the resisting moment of Section A can be expressed as:

$$M^A = \frac{E_c I \theta_A}{l_p^A} \tag{3}$$

where $l_p^A = \left[1 - 0.5(\rho - \rho')\frac{f_y}{f_c} - 0.5\frac{N}{f_c b h_0^A} \right] \cdot h_0^A$ is the equivalent length of plastic inflection at Section A suggested by Zhu et al. (1985). The support-induced membrane action (N and M) at Section A can be derived by:

$$N = \Delta \cdot S_n = \varepsilon l \cdot S_n \tag{4a}$$

$$M^A = \theta_s \cdot S_m = \frac{f}{lk} \cdot S_m \tag{4b}$$

where $S_n = [bh_i + \alpha_E(A_s + A'_s)]E_c/l$; $S_m = 1/\left(\frac{1}{Nl} - \frac{l_p^A}{E_c I}\right)$; $k = \frac{l_p^A S_m}{E_c I} + 1$; $bh_i + \alpha_E(A_s + A'_s)$ is the equivalent compression area of cross-section; $\alpha_E = E_s/E_c$; E_c and E_s are the elastic modulus of concrete and reinforcement, respectively; A'_s and A_s are the section areas of reinforcement in compression and tension zones, respectively; b is the section width; h_0^A is the effective height of Section A ; ρ and ρ' are the reinforcement ratios in tension and compression zones, respectively; f_y is the yield strength of reinforcement; f_c is the compressive strength of concrete; $h_i = h - \Delta h$ is the current section height and Δh is the crushed height of cross-section.

As depicted in Fig. 2, the load responses will experience a fluctuating path to the catastrophic collapse of the structural member. The stress-strain relationship

of the cross-section can be artificially divided into two stages (see Fig. 5): (i) the stress-strain distribution obeys Hooke's law, and a triangle stress distribution is achieved for concrete in the compression zone; (ii) reinforcing bars in both the tensile and compression zones yield as the load continues, and an equivalent rectangular stress distribution is suggested.

For state I displayed in Fig. 5a and c, the resisting moment of the cross-section can be written as:

$$M_R = 0.5\xi_n^2 h_0^2 b E_c \varphi \left(\frac{h}{2} - \frac{\xi_n h}{3} \right) + A'_s (\xi_n h_0 - a') E_s \varphi \left(\frac{h}{2} - a' \right) + A_s (1 - \xi_n) h_0 E_s \varphi \left(\frac{h}{2} - a \right) \tag{5}$$

where $\xi_n = \sqrt{[\alpha_E(\rho + \rho')]^2 + 2\left[\alpha_E(\rho + \rho')\frac{a'}{h_0} + \frac{N}{\varphi E_c b h_0^2}\right]} - \alpha_E(\rho + \rho')$ is the height coefficient of the compression zone; $\varphi = \xi_n h_0 \varepsilon_c$.

A plastic inflection with certain length forms at the mid-span as deflection progresses, and the height of compression zone is given by:

$$x = \xi_n h_0 = \frac{\frac{N}{b} + \rho f_y h_0 - \rho' f'_y h_0}{f_c} \tag{6}$$

Similarly, the resisting moment of the cross-section for state II shown in Fig. 5 (b) and (c) can be obtained by:

$$M_R = b f_c \xi_n h_i \frac{h_i - \xi_n h_i}{2} + f'_y A'_s \left(\frac{h_i}{2} - a' \right) + f_y A_s \left(\frac{h_i}{2} - a \right) \tag{7}$$

The deflection increases rapidly as plastic inflections develop. The bottom of Section A is compressed while the top is tensioned owing to the constraints of the clamped support, which is contrary to that obtained in

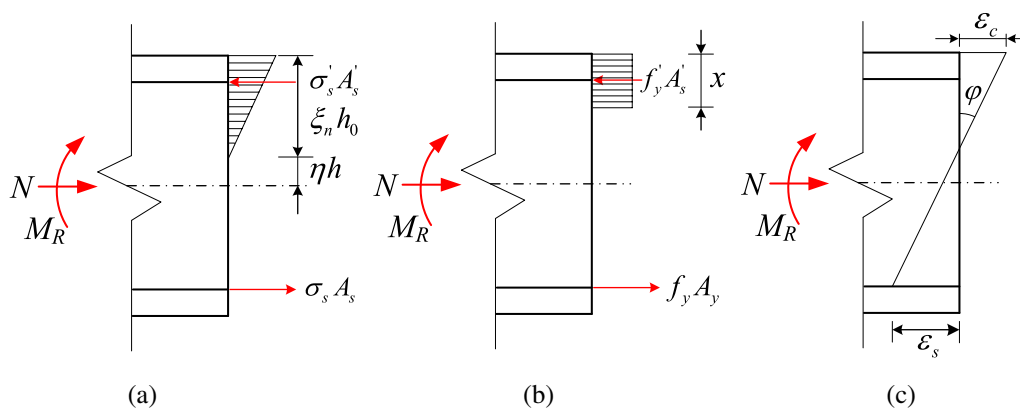


Fig. 5 Stress-strain distribution: a state I; b state II; c strain distribution

Section *B*. Consequently, the upwards movement of the neutral axis at Sections *A* and *B* can be derived by substituting Eq. (6) into $\eta h = 0.5h - \xi_n h_0$. Emphatically, a correction factor of $l_p^B = \left[1 - 0.5(\rho - \rho') \frac{f_y}{f_c} - 0.5 \frac{N}{f_c b h_0^B} \right] \cdot h_0^B$ is employed to express the equivalent length of plastic inflection at Section *B* (Zhu & Dong, 1985). The effective height of the cross-section can be derived by:

$$\eta^A h = 0.5h - \left(\frac{N}{bh_i^A} + \rho^A f_y - \rho^A f'_y \right) \frac{h_i^A}{f_c} \quad (8a)$$

$$\eta^B h = 0.5h - \left(\frac{N}{bh_i^B} + \rho^B f_y - \rho^B f'_y \right) \frac{h_i^B}{f_c} \quad (8b)$$

The resisting moments of Sections *A* and *B* are given as follows:

$$M_R^A = b f_c \xi_n^A h_i^A \frac{h - \xi_n^A h_i^A}{2} + f'_y A'_s \left(\frac{h}{2} - a' \right) + f_y A_s \left(\frac{h}{2} - a \right) \quad (9a)$$

$$M_R^B = b f_c \xi_n^B h_i^B \frac{h - \xi_n^B h_i^B}{2} + f'_y A'_s \left(\frac{h}{2} - a' \right) + f_y A_s \left(\frac{h}{2} - a \right) \quad (9b)$$

Commonly, the membrane action is a deflection-dependent load for clamped beam-like members. Consequently, the differentiation of the in-plane force with respect to deflection can be achieved as follows by substituting Eq. (4a) into Eq. (2).

$$\frac{dN}{df} = \frac{(\eta^A + \eta^B) \frac{h}{l} - \frac{\eta^A h}{lk} - \frac{f}{l}}{\left[\frac{l}{bh + \alpha_E (A_s + A'_s)} \right] E_c + \frac{1}{S_n}} \quad (\text{state I}) \quad (10a)$$

$$\frac{dN}{df} = \frac{h - (N^A + Z^A) \frac{h_i^A}{f_c} - (N^B + Z^B) \frac{h_i^B}{f_c} - f}{\left[\frac{\left(\frac{0.5h - h_i^A N^A + Z^A}{S_m} \right)^2}{S_m} + t + \frac{1}{S_n} \right] l} \quad (\text{state II}) \quad (10b)$$

where $N^A = \frac{N}{bh_i^A}$; $N^B = \frac{N}{bh_i^B}$; $Z^A = \rho^A f_y - \rho^A f'_y$; $Z^B = \rho^B f_y - \rho^B f'_y$ and $t = \frac{l}{[bh + \alpha_E (A_s + A'_s)] E_s}$.

As shown in Fig. 6, the ultimate resistance of the clamped beam under concentrated loading using membrane approach can be estimated by:

$$q = \frac{M_R^A + M_R^B - Nf}{l_1} = \frac{M_R^A + M_R^B - \frac{f}{lk} \cdot S_m}{l_1} \quad (11)$$

where l_1 is the distance between the concentrated load and Section *A*. For a simply supported beam, however, the ultimate resistance can be obtained as follows using

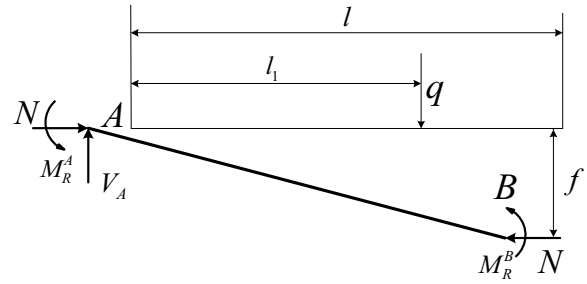


Fig. 6 Analytical model for half-span of the beam

the yield line approach recommended by Johansen (2004).

$$q_y = \frac{A_s f_y \left(h_0 - 0.59 A_s \frac{f_y}{f_c} \right)}{l_1} \quad (12)$$

As shown in Eq. (12), apparently, the ultimate load of the simply supported beam is an invariant value, which is relevant to the section dimension, reinforcement ratio and concrete strength but independent of the restraint stiffness of the support.

4 Model Validations

Familiarly, bending experiments are the popular and robust approach to examine the load response of beam-like members. Four-point bending tests based on orthogonal experimental theory have been conducted to inspect the impacts of deferring factors (including fibre content, reinforcement ratio and rod configuration) on the bearing capacities of clamped HFR-LWC beams (Chen et al., 2021), where the membrane contributions on ultimate resistance were intensively discussed.

To clarify this investigation, the experimental results previously provided by the author are cited to support the reliability and prediction accuracy of the proposed model. Emphatically, the information of specimen fabrication, test cases, measurement arrangement and failure appearances are slimmed down and highlight the novelty of this work. The cracking loads and the ultimate loads given by Chen et al. (2021) are listed in Table 1, in which the longitudinal restraint stiffness and rotational restraint stiffness for various rod configurations can be achieved by the published Eqs. (5) and (8a, 8b), respectively.

The cracking load and ultimate load are both important characteristic values for the load response of a beam-like member. The ultimate load-to-cracking load ratio is extremely valuable for assessing the ductility behaviour of the post-cracking branch. A larger ultimate load-to-cracking load ratio means that the

Table 1 Test results

Beam ID	$S_n(\text{N/mm})$	$S_m(\text{N mm/rad})$	$q'_e(\text{kN})$	$q_e(\text{kN})$	q_e/q'_e
A23	$2AE_s/L$	$8AE_s d^2/L$	32	184.0	5.75
A24	$4AE_s/L$	$6.4AE_s d^2/L$	24	128.0	5.33
A22	0	0	17	31.7	1.86
A53	$2AE_s/L$	$8AE_s d^2/L$	40	168.0	4.20
A66	$2AE_s/L$	$2AE_s d^2/L$	28	103.0	3.67
A64	$2AE_s/L$	0	24	64.0	2.66
A67	$4AE_s/L$	$6.4AE_s d^2/L$	32	124.0	3.87
A63	0	0	16	36.2	2.26
A61	$4AE_s/L$	$6.4AE_s d^2/L$	36	194.0	5.38
A62	0	0	24	51.0	2.12

q'_e is the experimental cracking load, and q_e is the experimental ultimate load.

structural member has better energy-absorption capacity and crack-resistance before its entire collapse. Different constraint strengths are achieved by altering the rod configurations in this paper. As previously confirmed (Chen et al., 2021), emphatically, the ultimate loads of the clamped beam would decrease somewhat owing to the participation of rod-③. A further investigation into the resistance contributions of the membrane effect found that the longitudinal force with rod configuration ①③ is diminished by 20% due to the decrease in rotational restraint stiffness. Accordingly, a reduction coefficient of 0.8 is reasonably suggested to consider the weakening effect of rod-③ on rotational restraint stiffness. The cracking loads and ultimate loads of ten specimens are summarized in Table 1. A deep inspection into the crack pattern indicates that beams A23, A53, A67 and A61 collapse with numerous bending cracks and several shear cracks, accompanied by a bursting noise lasting for a period of time (Chen et al., 2021). Bending failures are first observed in the tested beams, followed by bending-shear failures. The ultimate loads of beams A23, A53 and A61 are up to 184.0 kN, 168.0 kN and 194.0 kN, increasing by 480.44%, 364.09% and 280.39% compared with beams A22, A63 and A62, respectively. The larger ultimate load-to-cracking load ratios (ranging from 4.20 to 5.75) of the above beams than those of the other specimens illustrate that they collapse in a ductile manner, which can be well confirmed by the failure photos displayed in the (Chen et al., 2021). These phenomena illustrate that a stronger support constraint would give rise to a larger stress gradient near the beam ends and result in bending-shear failures. The ultimate load-to-cracking load ratio in beams A53, A66 and A64 demonstrates that the ductility of the clamped beam increases as the distance from the tie rod to the neutral axis decreases,

because the additional moment raised by longitudinal force is diminished by the reverse moment (i.e., the moment generated by rotational constraint). A larger ultimate load-to-cracking load ratio of 3.87 in beam A67 than 2.66 in beam A64 indicates that the toughness of the tested beam is further enhanced due to the participation of rod-①. In addition, the comparison of beams A53 and A67 indicates that the participation of rod-③ results in a slight increase in bending cracks and an evident decrease in ultimate resistance. The ultimate load-to-cracking load ratios of beams A22, A63 and A62 are only 1.86, 2.26 and 2.12, respectively, meaning that they have experienced a slight plastic deformation to their collapses. However, the ultimate load of beams A22, A63 and A62 decreases by 303.9%, 242.5% and 280.4% in comparison with beams A24, A67 and A62, respectively, indicating that the simply supported beam has a significantly lower load-carrying capacity compared with the clamped beam and undergoes a short path from the cracking load to its collapse. The pure bending failures with no spalled concretes at the top depicted in Chen et al. (2021) illustrate that more energy is absorbed before collapse, which is quite different from that in clamped beams. It can be concluded that the bearing capacities of clamped beams can be significantly enhanced by membrane action, and simultaneously, the ductility would be improved greatly, especially for beam members with strong rotational restraint stiffness.

(1) Resistance contributions of the boundary constraint

The results obtained by bending test and proposed model are both summarized in Table 2, in which the theoretical values are derived using Eqs. (11) and (12), respectively. In which, the resistance contributions of the membrane effect are scaled by the ratio of the ultimate load-to-yield line value.

Currently, there are no theoretical formulas can be used to estimate the compressive strength of LWC reinforced with two or more types of fibres. Libre et al. (2011) stated that polypropylene fibres exhibited similar effects on the pre-cracking behaviour of HFR-LWC compared with steel fibre. Therefore, the existing formula for steel fibre-reinforced LWC is employed to predict the compressive strength of polypropylene fibre reinforced-LWC. The empirical formula concerning enhancement coefficient, fibre content and aspect ratio recommended by Ye et al. (2020) is utilized to determine the compressive strength of HFR-LWC:

Table 2 Comparisons of theoretical value and experimental result

Beam ID	Reinf. ratio (%)	Rod-config	q_e (kN)	q_t (kN)	q_y (kN)	q_e/q_y	q_t/q_y	f (mm)	f/h
A23	0.28	①	184.0	170.7	34.63	5.31	4.93	14.5	0.073
A24	0.28	①③	128.0	126.4	34.63	3.67	3.65	7.4	0.037
A22	0.28	none	31.7	34.63	34.63	0.92	1.00	18.3	0.092
A53	0.28	①	168.0	165.6	34.65	4.85	4.78	7.8	0.039
A66	0.28	②	103.0	99.1	34.65	2.97	2.86	7.6	0.038
A64	0.28	③	64.0	61.7	34.65	1.85	1.78	10.7	0.054
A67	0.28	①③	124.0	121.6	34.65	3.58	3.51	17.3	0.087
A63	0.28	none	36.2	34.65	34.65	1.04	1.00	28.8	0.144
A61	0.42	①③	194.0	187.4	51.92	3.74	3.61	9.2	0.046
A62	0.42	None	51.0	51.92	51.92	1.00	1.00	22.0	0.117

q_e is the experimental ultimate load; q_t is the theoretical ultimate load; q_y is the yield line value; f is the peak experimental deflection and h is the section height.

$$f_c = \left(1 + \sum_{i=1}^2 \frac{\alpha_{ci} \varphi_{fi} l_{fi}}{d_{fi}} \right) \cdot f'_c \quad (13)$$

where α_c is the enhancement coefficient and set as 0.352; φ_f is the fibre content; l_f/d_f is the aspect ratio; f'_c is the compressive strength of LWC and the subscript i represents the fibre type. A compressive strength of 45.55 MPa is achieved using Eq. (13), which is slightly smaller than the measured value of 47.97 MPa because the hybrid effect of fibre is not reasonably considered in the formula.

The results listed in Table 2 indicate that the yield line capacities conform well to the experimental results of simply supported beam. A relative error of less than 2.0% between the yield line value and measured result is achieved, and thus, the relative ultimate load (defined as the ratio of the experimental ultimate load-to-yield line value (q_e/q_y) and theoretical ultimate load-to-yield line value (q_t/q_y) is reasonably employed to scale the resistance contributions of the membrane effect. Generally, the bearing capacities accompanying membrane action are obviously above the yield line values, with q_e/q_y ranging from 1.85 to 5.31 and q_t/q_y ranging from 1.78 to 4.93. In addition, the theoretical ultimate loads show remarkably good agreement with those of the bending test. The relative errors between the predicted load and measured value varying from 1.25 to 7.23% illustrate that the bearing capacities of the clamped beam can be estimated with a high level of accuracy. The deflection-hardening behaviours of the fibrous beam due to the addition of hybrid fibre are ignored in the analysis, which would lead to a slight discrepancy in the relative value between the theoretical model and bending test. The comparisons listed in Table 2 verify that the ultimate loads are intimately correlated to the rod configuration. Basically, a larger combined stiffness would result in a higher ultimate resistance. It is also found that the discrepancies in the ultimate load between the clamped beam and reference

beam tend to be apparent with peak deflection, illustrating that a larger deflection is conducive to the development of membrane action.

With respect to deflection, it is clear that the peak deflections of the reference beam increase greatly in comparison with the clamped beam. An increase of 147.30%, 278.94%, and 139.13% for the plain beam, fibrous beam with a reinforcement ratio of 0.28% and fibrous beam with a reinforcement ratio of 0.42%, respectively, is shown in Table 2. It can be concluded that the structural ductility would be diminished to a certain extent by the membrane effect, especially the longitudinal force produced by the rod combination ③. The reasons might be that the strong constraints of the clamped support give rise to a rapid climb of the bearing capacity but inevitably lead to sudden bending failure and even bending-shear failure if the deflection exceeds a certain value owing to the great stress gradients caused by the p - Δ effect (i.e., additional bending moment).

(2) Comparisons of applied load–deflection curves

Membrane action is activated by the boundary constraint associated with progressive deflection throughout the load-response stage. To quantitatively distinguish the discrepancies in resistance behaviour between the membrane approach and yield line approach, the variations of applied load versus deflection are discussed in this section. The applied load–deflection curves achieved by the proposed model and bending test are displayed in Fig. 7, where q/q_y denotes the ratio of the ultimate load-to-yield line value, and f/h is the relative deflection. All applied loads are greater than 1.0 when the deflections exceed a certain value, meaning that the membrane action is activated and has noticeable contributions to the ultimate resistance of tested beam. Generally, an ultimate load of 1.85 to 5.31 times the yield line value is obtained,

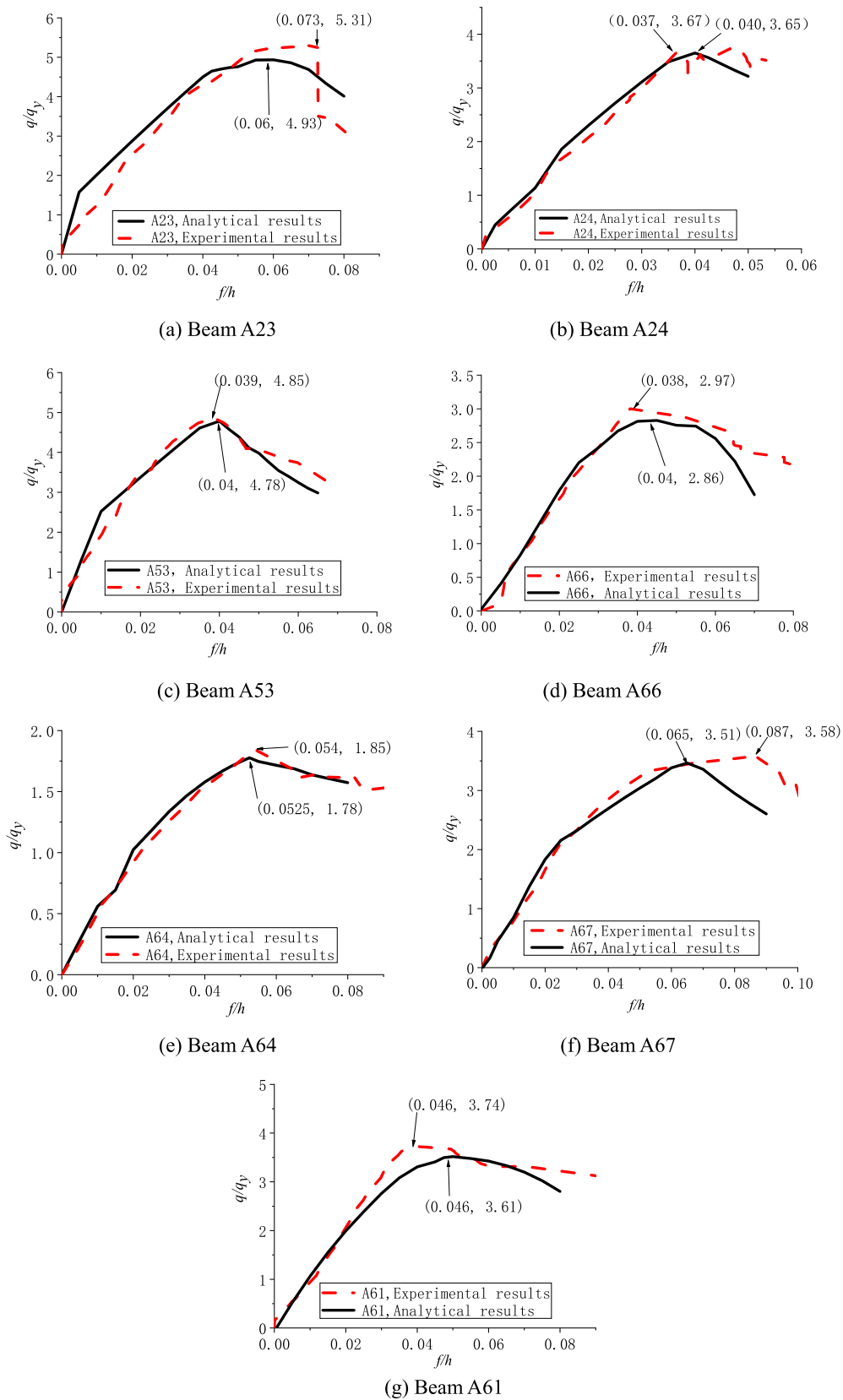


Fig. 7 Variations of applied load versus deflection

illustrating that the yield line approach will significantly underestimate the ultimate resistances of clamped beams. It is evident that the model predictions conform to the experimental results (either relative load or relative deflection) during the entire loading process. Nevertheless, a further analysis indicates that q_e/q_y is larger than q_t/q_y in the range from 0.5 to 7.7%. This phenomenon might result from the discrepancies in the material properties between the HFR-LWC and LWC, i.e., the post-cracking behaviour and deflection-hardening effect of the HFR-LWC are not considered in the theoretical analysis. In fact, the post-cracking behaviour of plain LWC can be enhanced by fibre addition. The interlocking effect of coarse aggregate and the bridging effect of hybrid fibre are significantly enhanced by membrane action, which also aids in increasing the response limit of the beam. The presence of hybrid fibres is helpful for stitching the macrocracks in the beam and permits the member to fail with fibre pull-out. Usually, the deflection-hardening behaviour can be observed in fibre-reinforced concrete if the first-peak strength is lower than the peak strength (Li et al., 2017b). Nevertheless, it is considerably difficult to distinguish the first peak point for materials with stable deflection-hardening behaviour, as stated by Kim et al. (2008). The first peak point is represented by the first cracking point in the current analysis based on the suggestions of Kim et al., (2008). Fig. 7 indicates that the first crack point of the tested beam increases greatly with the restraint stiffness of clamped support. However, the initial cracking point would experience a shorter path to the peak point with longitudinal restraint stiffness, illustrating that the membrane effect will result in a reduction of deflection-hardening behaviour. The ascending slope of the load–deflection curve increases with the distance from the tie rod to the neutral plane owing to the strong rotational restraint stiffness. Moreover, the descending branches of the load–deflection curve become smoother than those of the plain beam shown in Fig. 7. It is indicated that the fibre pulling-out failure aids in increasing the post-ductility performance of tested beam. In addition, a sudden truncation in the post-peak branch of the load–deflection curve is observed in Fig. 7b and f, meaning that the beam is collapsed in a brittle manner, which is also confirmed by the tensile force–deflection relationships. The inflated areas under the load–deflection curve of beams A23 and A67 demonstrate that much energy is absorbed by the pulling-out of the hybrid fibre before the specimen collapses.

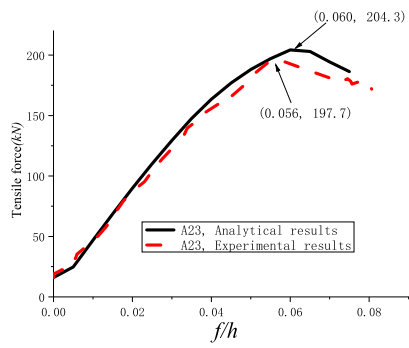
5 Impacts of Membrane Action

The impacts of membrane action on the load responses of clamped HFR-LWC beams are investigated. It is well known that the membrane effect is a

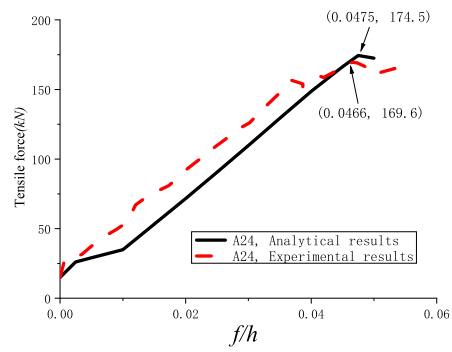
deflection-dependent action induced by clamped supports. The variations of longitudinal force (i.e., tensile force) versus relative deflection (a ratio of deflection-to-height) based on Eqs. (10a, 10b) are displayed in Fig. 8, in which the measured curves are also given. It is clear that the tensile forces obtained by the theoretical approach exhibit similar trends to those derived by the four-point bending tests. The maximum relative errors for the peak tensile force and corresponding deflection are only 9% and 19%, respectively. The high accuracy of the proposed model is validated by the good agreement between the model predictions and experimental results. Generally, the peak deflections of the fibrous beam are slightly underestimated by the theoretical approach if rod-③ is taken into account. The reasons might be that rod-③ produces a p- Δ effect on the beam at a larger deflection, which results in an additional deflection. The deflection increases linearly with tensile force before its peak value is reached. Moreover, the stronger the constraint strength is, the larger the slope of the tensile force–deflection curves. For example, the growth rate of the tensile force in beam A64 is smaller than that in beam A53 because only the outwards movement of beam A64 is prevented. Unlike beam A53, it is constrained by the in-plane force and resisting moment simultaneously. The gradual descending branches in the tensile force–deflection curves indicate that the tested beams collapse in a ductile manner. However, the sudden truncations in the descending branches of beams A24 and A67 demonstrate that they exhibit relatively poor ductile behaviour compared with clamped beams without rod-③.

An intensive investigation into the membrane contribution to the ultimate resistance of the HFR-LWC beam is given in Table 3, in which the membrane action is separated into N and M . It is evident that the predicted deflections exhibit similar longitudinal force and resisting moment dependencies as the experimental results. The largest relative deflection is achieved for beam A64, the beam with rod configuration ③. However, the relative deflection decreases rapidly as the resisting moment increases and reaches a minimum value for beam with rod configuration ①. The relative deflection of beam A67 increases slightly compared with beam A53 in both the predicted value and measured result, indicating that the participation of rod-③ seemingly produces a “negative” effect on the structural deflection response.

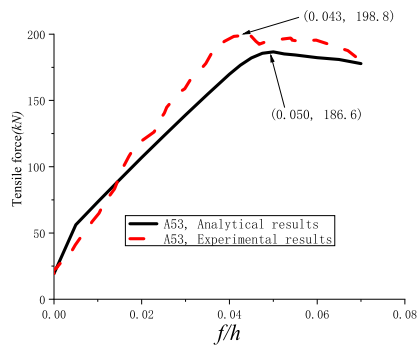
Fig. 9 shows that for a given fibre content and reinforcement ratio, the relative deflection of the beam tends to decrease significantly with the resisting moment. Nevertheless, this tendency is observed for beams with differing longitudinal forces, even if the relative deflection increases with the longitudinal force for the HFR-LWC beam with a similar resisting moment if rod-③



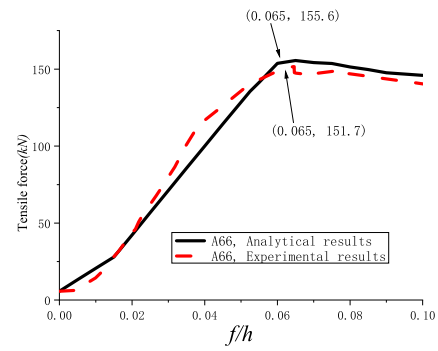
(a) Beam A23



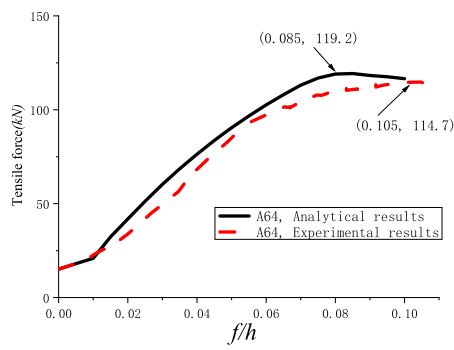
(b) Beam A24



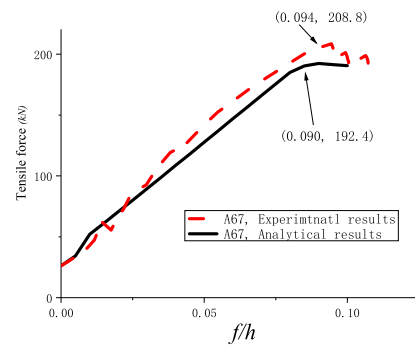
(c) Beam A53



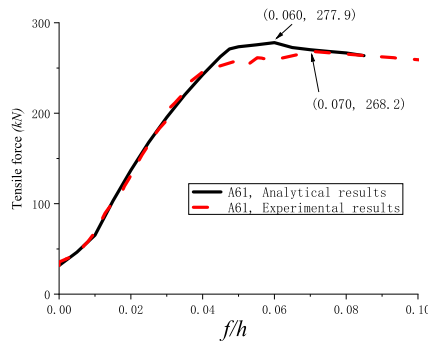
(d) Beam A66



(e) Beam A64



(f) Beam A67



(g) Beam A61

Fig. 8 Variations of tensile force versus deflection

Table 3 Comparisons of membrane action

Beam ID	Rod-conf	N_t (kN)	M_t (kN.m)	N_e (kN)	M_e (kN.m)	f'_t/h	f'_e/h
A23	①	204.3	16.34	197.7	15.82	0.060	0.056
A24	①③	174.5	8.07	169.6	7.84	0.048	0.047
A53	①	186.6	14.93	198.8	15.9	0.050	0.043
A66	②	155.6	6.22	151.7	6.07	0.065	0.065
A64	③	119.2	0.0	114.7	0.0	0.085	0.105
A67	①③	192.4	10.31	208.8	11.19	0.090	0.094
A61	①③	277.9	11.14	268.2	10.76	0.060	0.070

N_t and M_t are the peak values of theoretical in-plane force and resisting moment, respectively; N_e and M_e are the peak values of experimental in-plane force and resisting moment, respectively; f'_t/h is the theoretical deflection corresponding to N_t ; f'_e/h is the experimental deflection corresponding to N_e

participates in the rod configuration. This phenomenon demonstrates that the rotational restraint stiffness has a decisive effect on the deflection response of the beam, and the smallest deflection is achieved for a beam with rod configuration ① because the “inverted arch” effect, produced by the resisting moment, has a considerable effect on the deflection of the clamped beam and might never be surpassed by the p-Δ effect induced by the longitudinal force in certain conditions.

6 Conclusions

The resistance behaviours of HFR-LWC beam accompanying membrane action are theoretically investigated, and the reliabilities and prediction accuracies of proposed model are supported by experimental results. The following conclusions can be drawn:

- (1) The membrane effect is a combined action of the in-plane force and the resisting moment raised by clamped supports. The ultimate resistances of the

clamped beam can be significantly enhanced by the membrane effect, but simultaneously, the ductility would be diminished greatly, especially for a structure with a strong longitudinal constraint.

- (2) The relative loads exceed 1.0 when the deflections increase to a certain value, meaning that the membrane actions are activated and significantly contribute to the ultimate resistance of the HFR-LWC beam at large deflection. An ultimate load of 1.85 to 5.31 times the yield line value is generally achieved.
- (3) The relative errors between the predicted load and the measured value vary from 1.25% to 7.23%, illustrating that the bearing capacities of the clamped beam can be estimated with a high level of accuracy. The proposed model is capable of predicting the ultimate load of HFR-LWC beams accompanying membrane action and enriches the analytical model of RC member.
- (4) The resistance behaviours of HFR-LWC beam accompanying membrane action can be well depicted by the presented model. It is also suitable for the normal concrete beam with similar boundary constraints and applied loads, and thus presents a promising approach to estimate the bearing capacity of beam-like member in real-world situations.

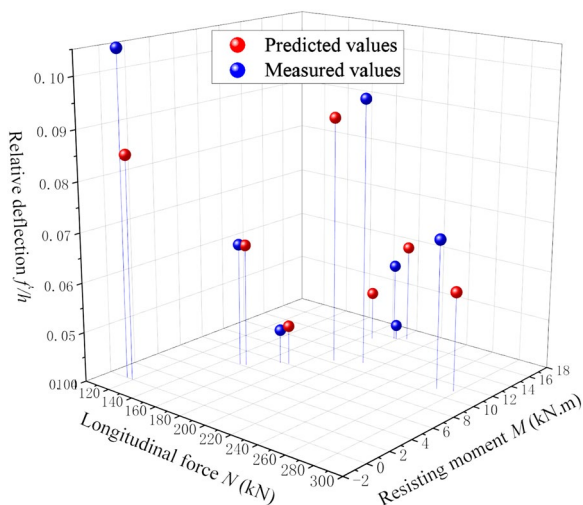


Fig. 9 Variations of deflection versus longitudinal force or resisting moment

Acknowledgements

We gratefully acknowledge the financial support from Basic Research Project (Grant: JCKY2020110C096), the National Natural Science Foundation of China (Grant: 52378548, 52278422), and the Natural Science Foundation of Jiangsu Province (Grant: BK20221530).

Author contributions

WC contributed to conceptualization, funding acquisition, investigation, resources, supervision, validation; JC wrote the manuscript; JH and XY performed the experiment; JM contributed to data analysis. All the authors read and approved the final manuscript.

Availability of data and materials

Some or all data, models, or code that support the findings of this study are available from the corresponding author upon reasonable request.

Declarations

Ethics approval and consent to participate

Not applicable.

Consent for publication

All the authors agree that the article will be published after acceptance. Informed consent was obtained from all individual participants included in this study.

Competing interests

There are no conflicts of interest with other reports or authors. The authors declare that they have no competing interests.

Received: 3 September 2023 Accepted: 11 November 2023

Published online: 22 February 2024

References

- Bailey, C. G. (2001). Membrane action of unrestrained lightly reinforced concrete slabs at large displacements. *Engineering Structures*, 23, 470–483.
- Bailey, C. G., White, D. S., & Moore, D. B. (2000). The tensile membrane action of unrestrained composite slabs simulated under fire conditions. *Engineering Structures*, 22, 1583–1595.
- Brotchie, J. F., & Holley, M. J. (1971). Membrane action in slabs: cracking, deflection and ultimate load of concrete slab systems, aci-30. *American Concrete Institute Detroit*, 30, 345–377.
- Burgess, I. (2017). Yield-line plasticity and tensile membrane action in lightly-reinforced rectangular concrete slabs. *Engineering Structures*, 138, 195–214.
- Chen, L., Fang, Q., Guo, Z., & Liu, J. (2014). An improved analytical method for restrained RC structures subjected to static and dynamic loads. *International Journal of Structural Stability and Dynamics*, 14(1), 1–35.
- Chen, W., & Guo, Z. (2010). Dynamic responses of reinforced concrete beams with viscous-spring supports subjected to low velocity impact. *Engineering Mechanics*, 27(5), 186–192.
- Chen, W., Luo, L., Guo, Z., & Wang, Y. (2020). Load-carrying capacities of fully-clamped RC slab accompanying compressive-tensile membrane actions: A theoretical approach. *International Journal of Structural Stability and Dynamics*, 20, 2050094.
- Chen, W., Luo, L., Guo, Z., & Yuan, P. (2021). Experimental studies on load-carrying capacity of HFR-LWC beam accompanying membrane action. *Engineering Structures*, 228(3), 111497.
- Fallah-Valukolaee, S., Hashemi, S. K., & Nematzadeh, M. (2022). Effect of steel fiber on flexural performance of bilayer concrete beams with steel and GFRP rebars: experiments and predictions. *Structures*, 39, 405–418.
- Gamble, W. L. (2000). *Reinforced concrete slabs* (2nd ed.). O the Oprah Magazine.
- Gillie, M., Usmani, A., & Rotter, M. (2004). Bending and membrane action in concrete slabs. *Fire and Materials*, 28, 139–157.
- Hognestad, E. (1953) Yield-line theory for the ultimate flexural strength of reinforced concrete slabs.
- Hossain-Zada, M. K., Kolagar, S., Fakoor, M., Vahedi, A., Nematzadeh, M., & Tabari, M. M. R. (2023). Post-heating flexural behavior of reinforced concrete beam with lap-spliced bar and feasibility of improving flexural performance by adding hybrid fibers. *Structures*, 55, 965–982.
- Hou, J., Shen, X., & Cui, Q. (2007). Study on physical and mechanical properties of hybrid fiber reinforced lightweight aggregate concrete. *New Building Materials*, 3, 80–83.
- Johansen, K. W. (1962). *Yield-line theory*. Cement and Concrete Association.
- Johansen, K. W. (2004). *Yield-line formulae for slabs*. Taylor and Francis.
- Kayali, O., Haque, M. N., & Zhu, B. (2003). Some characteristics of high strength fiber reinforced lightweight aggregate concrete. *Cement & Concrete Composites*, 25, 207–213.
- Kim, D. J., Naaman, A. E., & El-Tawil, S. (2008). Comparative flexural behavior of four fiber reinforced cementitious composites. *Cement and Concrete Composites*, 30, 917–928.
- Krauthammer, T. (2008). *Modern protective structures*. Taylor and Francis.
- Li, G., Zhou, H., & Guo, S. (2007). Mechanism and theoretical model of membrane action in slabs of steel buildings subjected to fire. *Journal of Building Structures*, 28(5), 40–47.
- Li, J., Niu, J., Wan, C., Liu, X., & Jin, Z. (2017b). Comparison of flexural property between high performance polypropylene fiber reinforced lightweight aggregate concrete and steel fiber reinforced lightweight aggregate concrete. *Construction and Building Materials*, 157, 729–736.
- Li, J., Wan, C., Niu, J., Wu, L., & Wu, Y. (2017a). Investigation on flexural toughness evaluation method of steel fiber reinforced lightweight aggregate concrete. *Construction and Building Materials*, 131(Jan30), 449–458.
- Libre, N. A., Shekarchi, M., Mahoutian, M., & Soroushian, P. (2011). Mechanical properties of hybrid fiber reinforced lightweight aggregate concrete made with natural pumice. *Construction and Building Materials*, 25, 2458–2464.
- Mo, K. H., Yeoh, K. H., Bashar, I. I., Johnson Alengaram, U., & Jumaat, M. Z. (2017). Shear behaviour and mechanical properties of steel fibre-reinforced cement-based and geopolymer oil palm shell lightweight aggregate concrete. *Construction and Building Materials*, 148, 369–375.
- Nematzadeh, M., & Hasan-Nattaj, F. (2017). Compressive stress-strain model for high-strength concrete reinforced with Forta-Ferro and steel fibers. *J Mater Civil Eng*, 29(10), 04017152.1-04017152.15.
- Nematzadeh, M., Hosseini, S.-A., & Ozbakkaloglu, T. (2021). The combined effect of crumb rubber aggregates and steel fibers on shear behavior of GFRP bar-reinforced high-strength concrete beams. *Journal of Building Engineering*, 4, 102981.
- Ockleston, A. J. (1955). Load tests on a three storey reinforced concrete building in Johannesburg. *Structure Engineering*, 33(10), 304–322.
- Pan, L., Yuan, H., & Zhao, S. (2011). Experimental study on mechanical properties of hybrid fiber reinforced full lightweight aggregate concrete. *Advanced Materials Research*, 197, 911–914.
- Park, R. (1964a). Tensile membrane behaviour of uniformly loaded rectangular reinforced concrete slabs with fully restrained edges. *Magazine of Concrete Research*, 16(46), 39–44.
- Park, R. (1964b). Ultimate strength of rectangular concrete slabs under short-term uniform loading with edges restrained against lateral movement. *Proc Inst Civil Eng*, 28, 125–150.
- Park, R., & Park, R. (1975). *Reinforced concrete structures/by R. Universitas Negeri Malang*.
- Qian, Q., & Wang, M. (2009). *Calculation theory for advanced protective structures*. Phoenix Science Press.
- Sabetifar, H., & Nematzadeh, M. (2021). An evolutionary approach for formulation of ultimate shear strength of steel fiber-reinforced concrete beams using gene expression programming. *Structures*, 34, 4965–4976.
- Shen, J., Wang, C., & Jiang, J. (1993). *Finite elements method of reinforced concrete and limit analysis of concrete slabs and shells*. Tsinghua University Press.
- Wang, D., Guo, Z. K., Shao, F., & Chen, W. (2014). Experimental study on dynamic mechanical properties of HPP hybrid fibers reinforced lightweight aggregate concrete. *Advanced Materials Research*, 919–921, 1983–1989.
- Wang, H., & Wang, L. (2013). Experimental study on static and dynamic mechanical properties of steel fiber reinforced lightweight aggregate concrete. *Construction and Building Materials*, 38, 1146–1151.
- Wood, R., Armer, G., & Montcrieff, M. (1970). Additional discussion: The theory of the strip method for design of slabs. *Ice Proceedings*, 46(3), 385.
- Ye, Y., Liu, J., Zhang, Z., Wang, Z., & Peng, Q. (2020). Experimental study of high-strength steel fiber lightweight aggregate concrete on mechanical properties and toughness index. *Advances in Materials Science and Engineering*, 2020(7), 1–10.
- Zhou, Y., Liu, X., Xing, F., Cui, H., & Sui, L. (2016). Axial compressive behavior of FRP-confined lightweight aggregate concrete: An experimental study and stress-strain relation model. *Construction and Building Materials*, 119, 1–15.
- Zhu, B., & Dong, Z. (1985). *Nonlinear analysis of RC structures*. Tongji University Press.

Publisher's Note

Springer Nature remains neutral with regard to jurisdictional claims in published maps and institutional affiliations.

Wanxiang Chen is an Associate Professor at School of Civil Engineering at Sun Yat-sen University. He awarded his PhD in disaster prevention and mitigation engineering at PLA University of Science and Technology, directed by academician Qihu Qian (winner of the National Highest Science Award in 2018), who mainly engaged in blast-resistance of major national infrastructure & protection of deep underground engineering since 2000.

Jiawen Cai is a master's Student at School of Civil Engineering at Sun Yat-sen University. Her research interests include deep water explosive load modelling and ground vibration characterisation.

Junxuan Huang is a Master Student at School of Civil Engineering at Sun Yat-sen University. His research interests focus on the study of protection of underground structures.

Xiaoyu Yang is a Master Student at School of Civil Engineering at Sun Yat-sen University. His research interests focus on the study of protection of underground structures.

Jianjun Ma is an Associate professor at School of Civil Engineering at Sun Yat-sen University. He mainly engaged in geotechnical and tunnelling research.

Submit your manuscript to a SpringerOpen[®] journal and benefit from:

- ▶ Convenient online submission
- ▶ Rigorous peer review
- ▶ Open access: articles freely available online
- ▶ High visibility within the field
- ▶ Retaining the copyright to your article

Submit your next manuscript at ▶ [springeropen.com](https://www.springeropen.com)
